Modeling cell size control using differential scaling of cell-cycle regulators with cell size

Xiangrui Ji[1], Jie Lin[2,3*]

1 Yuanpei College, Peking University, Beijing, China
2 Center for Quantitative Biology, Academy for Advanced Interdisciplinary Studies, Peking University, Beijing, China
3 Peking-Tsinghua Center for Life Sciences, Academy for Advanced Interdisciplinary Studies, Peking University, Beijing, China

* linjie@pku.edu.cn

Abstract

Accurate timing of division and size homeostasis is crucial for cells. A potential mechanism for cells to decide the timing of division is the differential scaling of regulatory protein copy numbers with cell size. However, it remains unclear whether such a mechanism can lead to robust growth and division, and how the scaling behaviors of regulatory proteins affect the cell size distribution. In this study, we formulate a mathematical model combining gene expression and cell growth, in which the cell-cycle inhibitors scale sublinearly with cell size while the activators scale superlinearly. The cell divides once the ratio of their concentrations reaches a threshold value. We find that the cell can robustly grow and divide within a finite range of the threshold value. Intriguingly, the cell size at birth is proportional to the ploidy, in agreement with experiments. In a stochastic version of the model, the cell size at division is uncorrelated with that at birth. Also, the more differential the cell-size scaling of the cell-cycle regulators is, the narrower the cell-size distribution is. Finally, after the deletion of a regulator, the average cell size can change significantly while the coefficient of variation of cell size remains roughly the same, consistent with experimental observations.

Author summary

How cells determine the timing of cell division is a fundamental question of cell biology. It has been found that the concentration of cell-cycle activators tends to increase with cell size, while the concentration of inhibitors tends to decrease. Therefore, an attractive hypothesis is that the ratio of activators to inhibitors may trigger cell division. To investigate this hypothesis quantitatively, we formulate a model including gene expression and cell growth simultaneously. The cell divides once the activator-to-inhibitor ratio reaches a threshold. Combining theories and simulations, we analyze the conditions of robust cell cycle and the cell size distribution. Our model successfully rationalizes several experimental observations, including the relation between cell size and ploidy, the sizer behavior of cell size control, and the change of the mean and fluctuation of cell size distribution after regulator deletion.

Introduction

Cells must coordinate growth and division to keep their sizes within a finite range, which is vital for various biological functions and cellular fitness. For example, a very large cell volume may remodel the proteome and trigger senescence [1, 2]. On the other hand, a very small cell volume may also reduce cellular fitness, which may be due to the limited protein copy numbers and the resulting large fluctuation in protein concentrations [3–5]. Therefore, cells must evolve ways to measure their sizes to accurately decide the timing of division. Recently, Chen et al. proposed that the timing of cell-cycle entry can be achieved through the differential scaling of cell-cycle regulators. If the activators exhibit superlinear scaling with cell size while the inhibitors exhibit sublinear scaling, then at some sufficiently large cell size, the activators dominate over the inhibitors and trigger cell-cycle entry [6]. This hypothesis is supported by the observations that the concentrations of many proteins change with cell size as the cell size increases [2, 7]. RNA sequencing also showed that the cell-cycle activators (inhibitors) are enriched in the subset of genes that exhibit increasing (decreasing) mRNA concentrations as the cell size increases [6]. While the mechanism of cell size control based on the differential scaling of cell-cycle regulators is plausible, it is unclear whether it leads to robust growth and division. More quantitatively, how does the differential scaling of regulators determine the cell size? The answers to these questions can deepen our understanding of cell-cycle regulation and cell size control.

Regarding the mechanisms of differential scaling, one of us has recently proposed a gene expression model at the whole-cell level in which the promoters of all genes compete for the resource of RNA polymerases (RNAPs) [8]. The model predicts that the effective binding affinities of promoters to RNAPs determine the nonlinear scaling of protein numbers vs. cell size. A gene with a relatively strong promoter exhibits a decreasing protein concentration as the cell size increases, while a gene with a relatively weak promoter exhibits the opposite behavior. The model suggests that the nonlinear scaling between protein numbers and cell size is an inevitable consequence of heterogeneous promoter strengths in the genome.

In this work, we formulate a model of cell size control combining the hypothesis of nonlinear scaling of cell-cycle regulators and the whole-cell gene expression model. The activators have weak promoters and therefore exhibit superlinear scaling with cell size. Meanwhile, the inhibitors have strong promoters and exhibit sublinear scaling. In the following, we first discuss the case of a single activator and a single inhibitor. When the ratio of the activator's concentration to the inhibitor's concentration rises to a threshold value θ, the cell divides (Fig 1A).

In the main text, we focus on the case where most proteins are nondegradable while the cell-cycle regulators are degradable, supported by the observations that most proteins are stable in yeast and the minority of short-lived proteins are mainly enriched in the cell cycle category [9]. Our conclusions are qualitatively similar for nondegradable cell-cycle inhibitors (S1 Appendix). We mainly consider a simple scenario with constant gene copy numbers, rationalized by imagining a cell that replicates its genes right before cell division. Therefore, the gene copy number is constant throughout the cell cycle. We also discuss a modified model in which the cell replicates its genes when the ratio of the activator to the inhibitor rises to a threshold and divides after a constant time (S1 Appendix). Our conclusions are qualitatively similar between the simple scenario and the modified model.

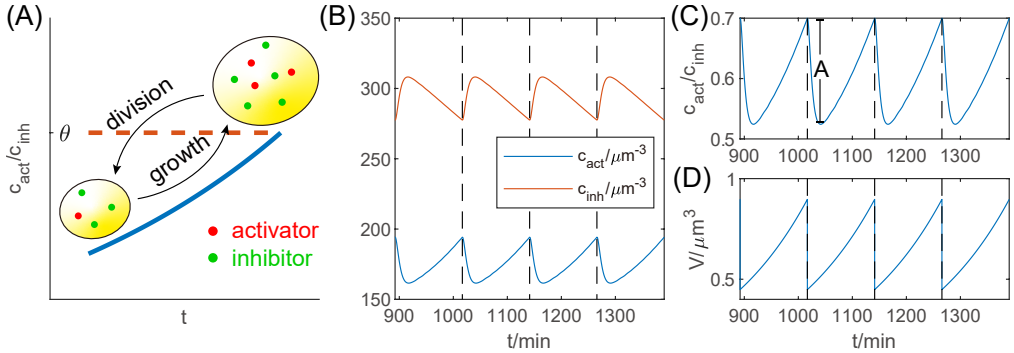

Fig 1. Periodic cell division in the simulations of the cell cycle model. (A) The cell divides symmetrically once the ratio of the activator's concentration to the inhibitor's concentration reaches a threshold value. We track one of the daughter cells and simulate a single lineage. (B) The periodic concentrations of the activator c_{act} and inhibitor c_{inh}. (C) The ratio $c_{\mathrm{act}}/c_{\mathrm{inh}}$ in the periodic steady state. A is the amplitude of the periodic oscillation. (D) The cell volume V also changes periodically. The abrupt drop corresponds to cell division. In (B-D), the dashed lines mark cell division. In this figure $K_{n,\mathrm{act}} = 12000\ \mu\mathrm{m}^{-3}$, $K_{n,\mathrm{inh}} = 4000\ \mu\mathrm{m}^{-3}$, and $\theta = 0.7$. The simulation details are in Methods.

Results

The model of cell-cycle regulation generates robust cell division

We model gene expression at the whole-cell level by explicitly incorporating the competition between genes for the resource of RNAPs and between mRNAs for the resource of ribosomes [8, 10]. A free RNAP can bind to the promoters and become an initiating RNAP, which can start transcribing or hop off the promoters without transcribing. Thus, the concentration of free RNAPs sets the transcription initiation rate through the Michaelis-Menten (MM) mechanism. The MM constant quantifies each gene's ability to recruit RNAPs. The time dependence of the mRNA copy number of one particular gene i is,

$$\frac{\mathrm{d}m_i}{\mathrm{d}t} = \Gamma_{n,i} g_i \frac{c_{n,\mathrm{free}}}{c_{n,\mathrm{free}} + K_{n,i}} - \frac{m_i}{\tau_{m,i}}, \tag{1}$$

where $c_{n,\mathrm{free}}$ is the free RNAP concentration in the nucleus and $K_{n,i}$ is the MM constant. A larger $K_{n,i}$ represents a weaker promoter, while a smaller $K_{n,i}$ represents a stronger promoter. g_i is the copy number of gene i and $\tau_{m,i}$ is the corresponding mRNA lifetime. $\Gamma_{n,i}$ is the rate for a promoter-bound RNAP to become a transcribing RNAP. Interaction between genes due to the limiting resource of RNAPs is through the free RNAP concentration. For one copy of each gene, the number of actively transcribing RNAPs is proportional to the probability that its promoter is bound by an RNAP, based on the assumption that the number of RNAPs starting transcription per unit time is equal to the number of RNAPs finishing transcription per unit time. This assumption is justified by the fact that it usually takes shorter than one minute for an RNAP to finish transcribing a gene [11] so that the system can quickly reach a steady state that does not change with time.

Using the conservation of the total RNAP number, we can find the free RNA concentration self-consistently (Eq 8). We introduce the relative fraction of free RNAPs in total RNAPs F_n such that $c_{n,\mathrm{free}} = c_n F_n$ where c_n is the concentration of total RNAPs in the nucleus. Details of the gene expression model are included in Methods

and also in [8]. A similar model as Eq 1 applies to the protein number (Eq 7), in which the free ribosome concentration sets the initiation rate of translation. In this work, we assume that the cell size is simply proportional to the total protein mass, supported by experiments [12–15] (see model details in Methods).

It has been shown that the MM constant $K_{n,i}$ determines the nonlinear scaling of protein number with cell size [8]. For genes with $K_{n,i}$ larger than the average MM constant, their protein numbers exhibit superlinear scaling with cell size and, therefore, an increasing concentration as the cell grows. Meanwhile, for genes with $K_{n,i}$ smaller than the average MM constant, their protein numbers exhibit sublinear scaling with cell size and, therefore, a decreasing concentration as the cell grows. The relation between the promoter strength and nonlinear scaling of protein level raises the possibility that cell-cycle inhibitors may have strong promoters while activators may have weak promoters [8]; thus, the ratio of their concentrations depends on cell size and allows a cell to determine its size and decide when to divide [6].

In the following, we first consider a model with one activator and one inhibitor. The transcription MM constants of the activator and inhibitor are respectively $K_{n,\mathrm{act}}$ and $K_{n,\mathrm{inh}}$ ($K_{n,\mathrm{act}} > K_{n,\mathrm{inh}}$), while the MM constants of other genes are equal to K_n for simplicity. Later, we will generalize the model to the case of multiple activators and inhibitors. The cell divides once the ratio of the activator's concentration to the inhibitor's concentration rises to the threshold value,

$$\frac{c_{\mathrm{act}}}{c_{\mathrm{inh}}} = \theta. \tag{2}$$

We numerically confirm that the cell can indeed reach a steady state, growing and dividing periodically (Fig 1B-D, see Methods for the simulation details). There is a transient increase in the inhibitor concentration and a transient decrease in the activator concentration. This is because of the reduced RNAP number at cell birth compared to cell division. The fewer total RNAP number leads to fewer free RNAPs given the same gene copy number. This means a decreasing concentration of free RNAPs right after cell division (S1 Fig). The initial low concentration of free RNAPs lets the inhibitor increase faster than other proteins because of its strong promoter, leading to an increasing inhibitor concentration. However, the advantage of the inhibitor over other proteins becomes weaker as the free RNAP concentration increases since all promoters are fully saturated in the limit of very high free RNAP concentration. Therefore, the inhibitor's concentration decreases as the cell grows. The opposite situation applies to the activator. After the transient regime, $c_{\mathrm{act}}/c_{\mathrm{inh}}$ increases, eventually reaches the threshold θ and triggers cell division (Fig 1C-D) (see more detailed analysis in Methods). We note that the transient decrease of $c_{\mathrm{act}}/c_{\mathrm{inh}}$ at the beginning of cell cycle is abrupt in the limit of short lifetimes of mRNAs and regulatory proteins (S1 Appendix).

Stable cell cycle exists between two critical division thresholds

One of our ultimate goals is to understand how cell size depends on the scaling behaviors of the cell-cycle regulatory proteins. We successfully derived the expression of the cell size at cell birth V_b (see details in Methods). The essence is to find the RNAP number at birth n_b. Because the total RNAP concentration c_n is essentially constant, one immediately obtains

$$V_b = \frac{a n_c (1-\theta)\tilde{K}}{2((1-\theta)c_n - \tilde{K})((1-\theta)K_n + \tilde{K})}, \tag{3}$$

where $\tilde{K} \equiv \theta K_{n,\mathrm{act}} - K_{n,\mathrm{inh}}$. Here a is the ratio between the cell volume and the nuclear volume, which is approximately constant, supported by experiments [16, 17]. n_c

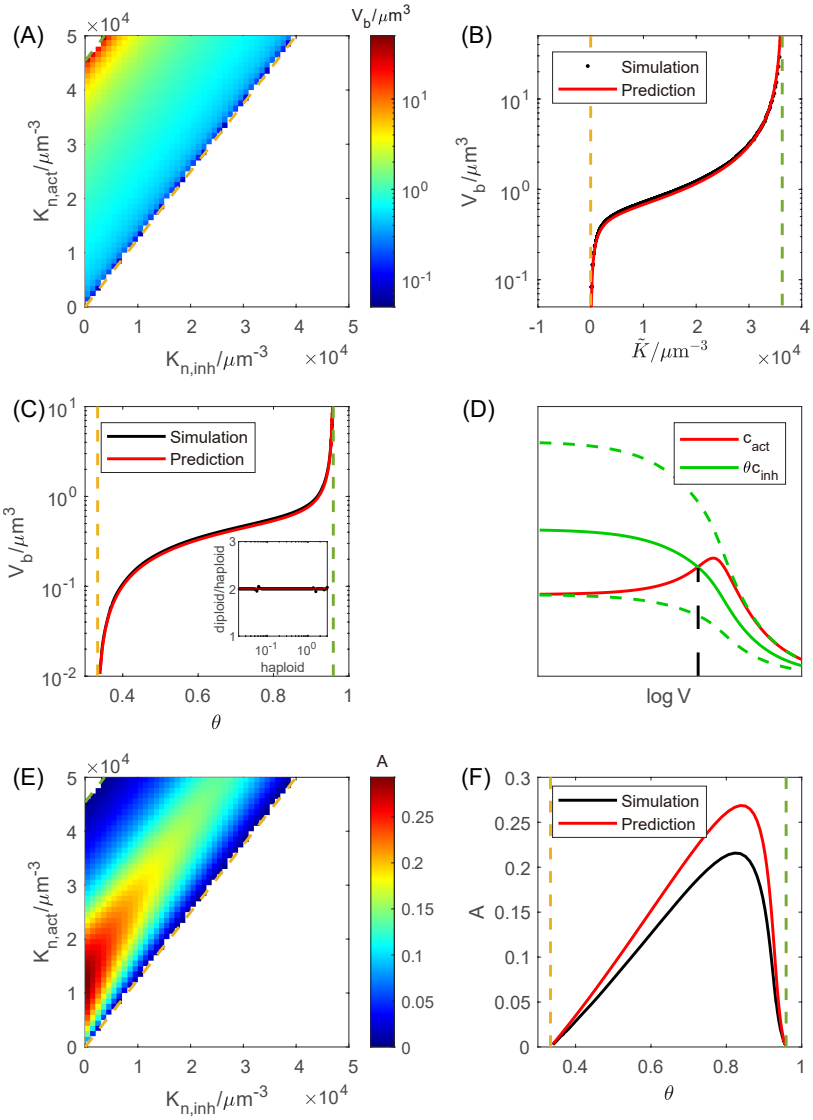

Fig 2. Simulations and theoretical predictions of the cell cycle model. (A) The heatmap of V_b as a function of $K_{n,\mathrm{act}}$ and $K_{n,\mathrm{inh}}$. The striped color gradient suggests that V_b is a function of a linear combination of $K_{n,\mathrm{act}}$ and $K_{n,\mathrm{inh}}$. (B) Simulations and theoretical predictions of V_b vs. $\tilde{K} \equiv \theta K_{n,\mathrm{act}} - K_{n,\mathrm{inh}}$. The simulation data here are the same as those in (A). (C) Simulations and theoretical predictions of V_b vs. θ. Inset: the ratio between the V_b's of diploid and haploid cells vs. V_b of the haploid cell. The diploid cell size is twice the haploid. Each point corresponds to a given θ. (D) Illustration of the origins of the two critical points. The intersection of c_{act} and θc_{inh} determines the cell size at division V_d. Beyond the two critical threshold values (dashed lines), there is no intersection. Between the two critical threshold values, as θ increases, the intersection shifts right so that V_d increases with θ. (E) The heatmap of A as a function of $K_{n,\mathrm{act}}$ and $K_{n,\mathrm{inh}}$. (F) Simulations and theoretical predictions of A as a function of θ. In (A, B, E), $\theta = 0.8$. In (C, F), $K_{n,\mathrm{act}} = 12000$ μm^{-3}, $K_{n,\mathrm{inh}} = 4000$ μm^{-3}. The dashed lines in (A-C, E, F) mark the two predicted critical threshold values.

is the maximum number of RNAPs that the entire genome can hold (Eq 19). Intriguingly, we find that V_b only depends on $\tilde{K}$, a linear combination of $K_{n,\mathrm{act}}$ and

$K_{n,\text{inh}}$ (Fig 2A-B). The comparison between the predictions and simulations shows good agreement (Fig 2B-C). We find that the solution is biologically meaningful only when the numerator and denominator of Eq 3 are positive, which is equivalent to requiring the fraction of free RNAPs to satisfy $0 < F_n < 1$ (Methods). Therefore, $\tilde{K}$ must satisfy

$$0 < \tilde{K} < (1-\theta)c_n, \tag{4}$$

from which we obtain the conditions of a stable cell cycle,

$$\frac{K_{n,\text{inh}}}{K_{n,\text{act}}} < \theta < \frac{c_n + K_{n,\text{inh}}}{c_n + K_{n,\text{act}}}. \tag{5}$$

The cell can grow and divide within a finite range of θ. The two critical threshold values $\theta_1 = \frac{K_{n,\text{inh}}}{K_{n,\text{act}}}$ and $\theta_2 = \frac{c_n+K_{n,\text{inh}}}{c_n+K_{n,\text{act}}}$ respectively set the lower bound and the upper bound. The predictions of a finite range of θ for a stable cell cycle are consistent with simulations (Fig 2A-C).

We provide an intuitive picture of the critical threshold values in the following. We note that the inhibitor's concentration keeps decreasing as the cell size increases since its advantage over other proteins becomes weaker and weaker with the increasing concentration of free RNAPs. The activator's concentration first increases as we predict. However, when the cell size is so big that genes get saturated by RNAPs, and mRNAs get saturated by ribosomes, the protein production rates will also reach their maximum values, which is called Phase 3 of gene expression in [10]. Mathematically, this corresponds to the situation in which the free RNAP concentration is above most genes' transcription MM constants (Eq 1) and the free ribosome concentration is above most mRNAs' translation MM constants (Eq 7). Thus, the protein numbers of the degradable activator and inhibitor both become constant, and their concentrations decrease inversely with the cell size in the large cell size limit. Therefore, for the two curves of c_{act} and θc_{inh} to cross, the threshold θ must be within a finite range (Fig 2D). In the modified model incorporating gene replication (S1 Appendix and S6 Fig), we only need to slightly modify the expression of V_b, and the two critical threshold values remain the same. For the case of nondegradable inhibitor, we also derived V_b and provided an illustration for the critical threshold values (S1 Appendix and S7 FigA-B).

We define A as the amplitude of the oscillation of $c_{\text{act}}/c_{\text{inh}}$, i.e., the difference between θ and the minimum of $c_{\text{act}}/c_{\text{inh}}$ in one cell cycle (Fig 1C). We find that the amplitude A approaches 0 as θ approaches the two critical threshold values (Fig 2E-F). The critical point θ_1 corresponds to $F_n \to 0$ at cell division (see details in Methods). In this limit, the relative fraction of free RNAPs at cell birth also approaches zero since the RNAP number decreases after cell division. The critical point θ_2 corresponds to $F_n \to 1$ at cell division (Methods). In this limit, almost all RNAPs are free, which means that the genes are fully saturated by RNAPs at cell division, and therefore F_n is still close to 1 at cell birth. In both cases, the F_n at cell birth is close to the F_n at cell division. On the other hand, we note that the minimum value of $c_{\text{act}}/c_{\text{inh}}$ is set by the F_n at cell birth (Eq 22), and the maximum value of $c_{\text{act}}/c_{\text{inh}}$, which is always equal to θ, is set by F_n at cell division. Therefore, the amplitude A approaches 0 as θ approaches the two critical threshold values. We derived an approximate expression of A (Methods), which agrees well with simulations (Fig 2F). Later we will show that the magnitude of A is crucial for a stable cell cycle when the threshold θ is subject to noise.

The cell size at birth is proportional to the ploidy

It is well known that the cell size is usually proportional to the ploidy [18–20]. Previous hypotheses about this observation were reviewed in [21, 22]. Our model provides a new perspective on the linear relationship between cell size and ploidy. We remark that our

model is invariant as long as the size-to-ploidy ratio is constant. This can be seen from Eq 8 where the doubling of cell size and gene copy numbers leaves the fraction of free RNAPs F_n invariant. Note that the above argument requires that the RNAP concentration c_n is independent of ploidy, which is true in our model (Eq 14) and also supported by experiments [2]. Therefore, the ratio $c_{\mathrm{act}}/c_{\mathrm{inh}}$ in a diploid cell is the same as that in a haploid cell as long as the size of the diploid cell is twice the size of the haploid cell. Thus, the cell volume at birth V_b doubles in the diploid cell relative to the haploid cell (Fig 2C). This can also be seen from Eq 3, where n_c, the total number of RNAPs that can simultaneously bind to the genome, is proportional to ploidy (see Eq 19).

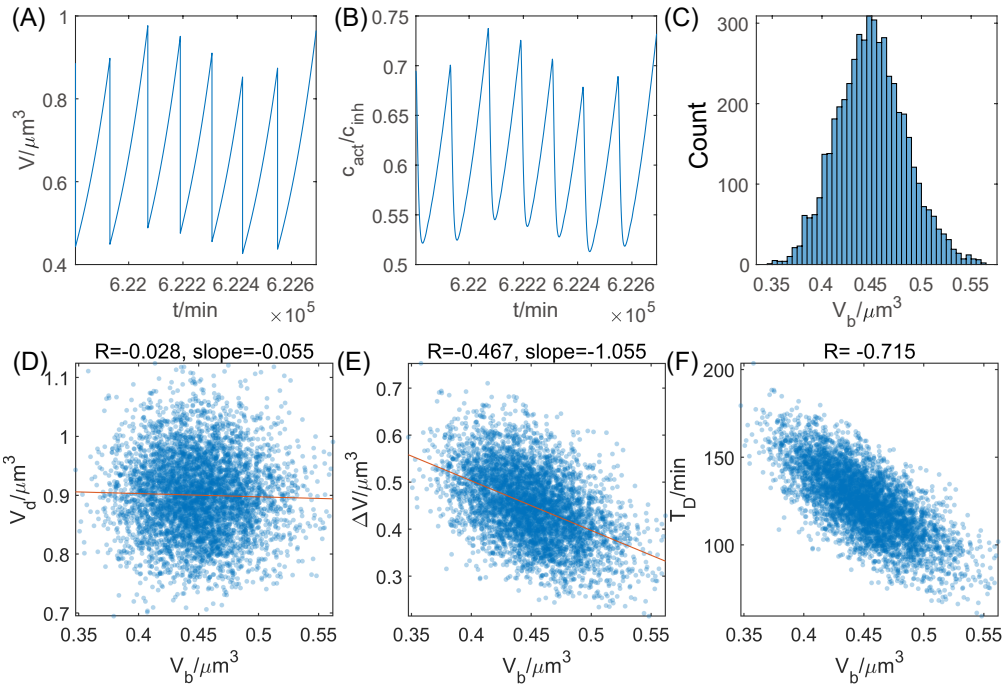

Fig 3. Simulations of the stochastic cell cycle model. (A) The time trajectory of cell size V. The cell can grow and divide sustainably. (B) The time trajectory of $c_{\mathrm{act}}/c_{\mathrm{inh}}$. (C) The distribution of cell size at birth V_b. (D) V_d vs. V_b. (E) ΔV vs. V_b. (F) T_D vs. V_b. In (D-F), each point represents one cell cycle. The Pearson correlation coefficient R and the slope of the linear regression are shown in the title. In all panels, $K_{n,\mathrm{act}} = 12000\ \mu\mathrm{m}^{-3}$, $K_{n,\mathrm{inh}} = 4000\ \mu\mathrm{m}^{-3}$, θ follows a normal distribution $N(\bar{\theta}, (\Delta\theta/3)^2)$, where $\bar{\theta} = 0.7$, $\Delta\theta = 0.1$. If $\theta \notin (\bar{\theta} - \Delta\theta, \bar{\theta} + \Delta\theta)$, we reset it as $\bar{\theta}$.

The cell cycle model with stochastic division threshold reveals a sizer behavior

We extend the model by adding noise to the division threshold θ to mimic randomness in real biological systems [3–5]. We assume that the threshold of each generation is independent and identically distributed. Since the threshold value is unlikely to be zero or infinite in real biological systems, we assume θ to be within a finite interval $(\bar{\theta} - \Delta\theta, \bar{\theta} + \Delta\theta)$ where $\bar{\theta}$ is the mean value. For a given parameter set, we simulate 5000 generations and trace one of the two daughter cells after symmetric division (Fig 3A-C). Intriguingly, we find that the cell size at division V_d is uncorrelated with the cell size at birth V_b (Fig 3D), in concert with the sizer behavior found in experiments [23–25].

Therefore, $\Delta V \equiv V_d - V_b$ and the doubling time T_D are negatively correlated with V_b (Fig 3E-F). The sizer behavior is robust against the parameter $\bar{\theta}$ (Fig 4A). This can be seen from Eq 3, where the cell size at cell birth is independent of that of the previous cell cycle. Intuitively, the sizer behavior is due to the degradation of the regulatory proteins: their numbers mainly depend on the current cell size and are insensitive to the history. Sizer due to the fast degradation of cell-cycle regulators is also proposed in [26]. We also studied the correlation between V_d and V_b for the case of nondegradable inhibitor and found an approximately zero correlation between V_d and V_b (S1 Appendix and S7 FigC-E).

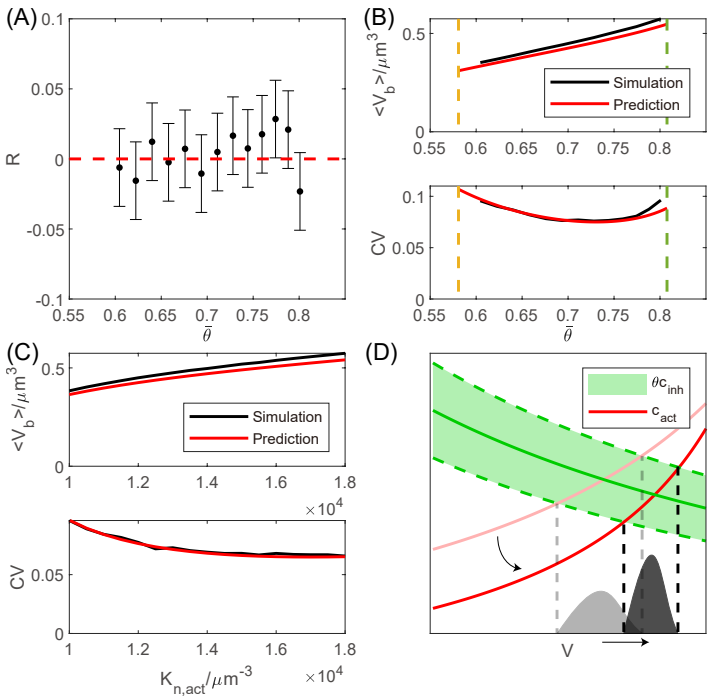

Fig 4. Comparison between theories and simulations of the stochastic model. (A) The Pearson correlation coefficient R between V_d and V_b is close to 0 for a range of $\bar{\theta}$. The error bars are the lower and upper bounds for a 95% confidence interval. (B) The average and CV of the cell size at birth V_b for a range of $\bar{\theta}$. The dashed lines mark the predicted critical threshold values in the presence of noise. In (A-B), $K_{n,\mathrm{act}} = 12000\ \mu\mathrm{m}^{-3}$, $K_{n,\mathrm{inh}} = 4000\ \mu\mathrm{m}^{-3}$. (C) $\langle V_b \rangle$ increases with $K_{n,\mathrm{act}}$, and the CV of V_b decreases with $K_{n,\mathrm{act}}$. $K_{n,\mathrm{inh}} = 4000\ \mu\mathrm{m}^{-3}$, $\bar{\theta} = 0.7$, $\Delta\theta = 0.1$. $\langle V_b \rangle$ and the CV of V_b as functions of $K_{n,\mathrm{inh}}$ are shown in S2 FigA. (D) The intersection of c_{act} and $\bar{\theta} c_{\mathrm{inh}}$ (solid green line) determines the mean cell size at division $\langle V_d \rangle$. The intersections of c_{act} with $(\bar{\theta} + \Delta\theta) c_{\mathrm{inh}}$ and $(\bar{\theta} - \Delta\theta) c_{\mathrm{inh}}$ (green dashed lines) set the range of V_d. If $K_{n,\mathrm{act}}$ increases, the number of activator becomes more superlinear as a function of cell size, and c_{act} shifts to the red line with lower transparency. Therefore, $\langle V_d \rangle$ increases while the CV of V_d decreases. Since V_b is half of the V_d of the previous cell cycle, we immediately obtain the distribution of V_b. A similar schematic when $K_{n,\mathrm{inh}}$ changes is shown in S2 FigB.

Differential scaling behaviors of the activator and inhibitor narrow cell size distribution

Moreover, we derived the analytical expressions of the mean cell size at birth and the coefficient of variation (CV) of cell size at birth (see details in Methods). The predictions agree well with the simulations under various $\bar{\theta}$, $K_{n,\mathrm{act}}$ and $K_{n,\mathrm{inh}}$ (Fig 4B-C, S2 FigA). We note that when $K_{n,\mathrm{act}}$ increases or $K_{n,\mathrm{inh}}$ decreases, the $\langle V_b \rangle$ increases while the CV of V_b decreases, which can be intuitively understood from the cell-size dependence of c_{act} and c_{inh} (Fig 4D and S2 FigB). Since $K_{n,\mathrm{act}}$ and $K_{n,\mathrm{inh}}$ determine how nonlinear the activator and inhibitor are relative to the cell size, this observation suggests that the more differential the scaling behaviors of the cell-cycle regulators are, the smaller the CV of the cell size distribution is.

In the presence of noise, the range of threshold that allows robust cell growth and division becomes smaller. We find that the mean threshold $\bar{\theta}$ must satisfy (Methods)

$$A(\bar{\theta} + \Delta\theta) > 2\Delta\theta. \tag{6}$$

When $\Delta\theta = 0$, Eq 6 becomes $A(\theta) > 0$, which is precisely the condition of robust division for the deterministic model. We note that $\langle V_b \rangle$ can not approach zero or infinity in the presence of noise (Fig 4B), in contrast to the deterministic model. This result suggests that too small or too large cell size is unstable against noise, and cell size must stay in an appropriate range.

Multiple regulators render robust cell size distribution against gene deletion

Experimentally, it has been found that deleting one regulator's gene of the budding yeast *Saccharomyces cerevisiae* can change the mean cell size significantly, but the CV of cell size is approximately the same before and after deletion [6, 27] (S3 Fig). This suggests that there should be multiple cell-cycle regulators working in concert. To explore the influence of gene deletion, we extend the model to multiple activators and inhibitors. Each regulator has one gene copy, and the numbers of activators and inhibitors are respectively g_{act} and g_{inh}. We assume that all the activators' promoters have the same effective binding affinity to RNAPs, i.e., $K_{n,\mathrm{act}}$, and all the inhibitors' promoters have the same effective binding affinity to RNAPs, i.e., $K_{n,\mathrm{inh}}$. The cell divides once the ratio between the concentration of all activators and the concentration of all inhibitors reaches the threshold θ, i.e., $\frac{g_{\mathrm{act}} c_{\mathrm{act}}}{g_{\mathrm{inh}} c_{\mathrm{inh}}} = \theta$, where c_{act} (c_{inh}) is the concentration of a particular activator (inhibitor). Therefore, we define the equivalent threshold as $\tilde{\theta} \equiv \frac{g_{\mathrm{inh}}}{g_{\mathrm{act}}}\theta$ such that the division condition becomes $\frac{c_{\mathrm{act}}}{c_{\mathrm{inh}}} = \tilde{\theta}$. Therefore, all the results above hold as long as we substitute θ with $\tilde{\theta}$ in the deterministic model and substitute $\bar{\theta}$ and $\Delta\theta$ with $\frac{g_{\mathrm{inh}}}{g_{\mathrm{act}}}\bar{\theta}$ and $\frac{g_{\mathrm{inh}}}{g_{\mathrm{act}}}\Delta\theta$ in the stochastic model.

After deleting one activator, the equivalent threshold changes to $\frac{g_{\mathrm{inh}}}{g_{\mathrm{act}}-1}\theta$, which is larger than the wild type (WT) value $\frac{g_{\mathrm{inh}}}{g_{\mathrm{act}}}\theta$. Because V_b increases with θ (Fig 2C), the V_b of *activator*Δ is larger than WT, verified by simulations (Fig 5A). In the model of stochastic θ, $\langle V_b \rangle$ is also larger after the deletion of one activator (Fig 5B), consistent with experiments [6, 27, 28]. A similar analysis applies to inhibitor deletion. The cell volume becomes smaller after inhibitor deletion (Fig 5A-B). We find that in the range of $\bar{\theta}$ that simultaneously allows WT, *activator*Δ and *inhibitor*Δ to divide periodically, the CVs of these strains are very close (Fig 5B). Indeed, there exists a range of viable $\bar{\theta}$ such that the relative change of CV is smaller than that of $\langle V_b \rangle$ after regulator deletion (Fig 5C, S4 FigA), consistent with experiments [27]. For the case of nondegradable inhibitors, the results are qualitatively the same (S7 FigF-I). In Fig 5D and S4 FigB, we demonstrate schematically why the change in CV is typically small. The redundancy of

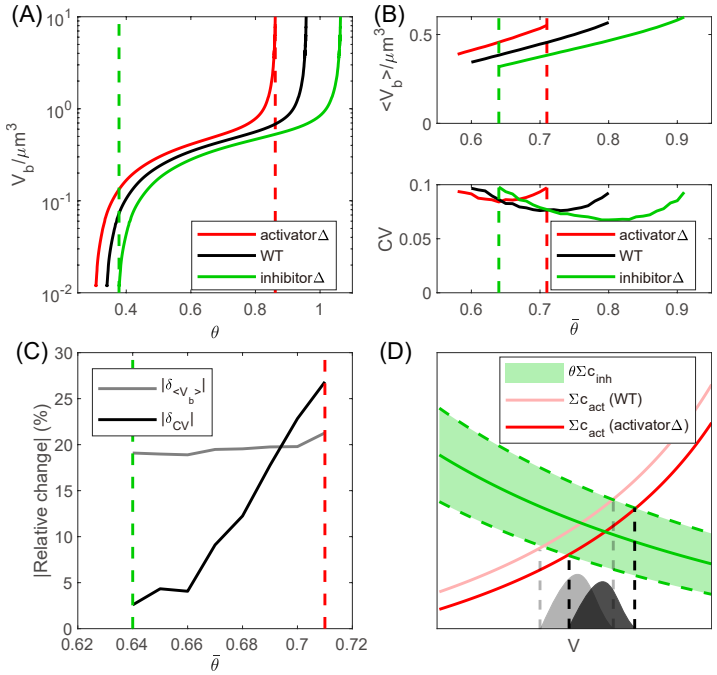

Fig 5. Simulations of multiple regulators. (A) Given a fixed θ, V_b increases after deleting one activator and decreases after deleting one inhibitor. The dashed lines mark the range of θ that simultaneously allows WT, *activator*Δ and *inhibitor*Δ to divide. (B) In the stochastic model, $\langle V_b \rangle$ increases after deleting one activator and decreases after deleting one inhibitor. The CV of V_b changes mildly after deleting one regulator. The dashed lines mark the range of $\bar{\theta}$ that simultaneously allows WT, *activator*Δ and *inhibitor*Δ to divide. (C) The absolute value of the relative change $\delta_{\langle V_b \rangle} \equiv \frac{\langle V_{b,\mathrm{act}\Delta} \rangle - \langle V_{b,\mathrm{WT}} \rangle}{\langle V_{b,\mathrm{WT}} \rangle}$ and $\delta_{\mathrm{CV}} \equiv \frac{\mathrm{CV}_{\mathrm{act}\Delta} - \mathrm{CV}_{\mathrm{WT}}}{\mathrm{CV}_{\mathrm{WT}}}$ after deleting one activator. The dashed lines have the same meaning as panel (B). Results of inhibitor deletion are shown in S4 FigA. In (B-C), $\Delta\theta = 0.1$. $K_{n,\mathrm{act}} = 12000\ \mu\mathrm{m}^{-3}$, $K_{n,\mathrm{inh}} = 4000\ \mu\mathrm{m}^{-3}$, $g_{\mathrm{act}} = g_{\mathrm{inh}} = 10$. (D) The deletion of one activator shifts the total concentration of all activators ($\sum c_{\mathrm{act}}$) downward while the total concentration of all inhibitors ($\sum c_{\mathrm{inh}}$) remain the same. This leads to a change in the mean cell size at division $\langle V_d \rangle$ while the CV of V_d is almost the same.

multiple regulators reduces the influence of deleting one cell-cycle regulator on the width of cell size distribution.

Discussion

In this work, we formulate a model combining cell size control and the differential scaling of gene expression with cell size. As the cell grows, the ratio between the activator and inhibitor increases and eventually triggers cell division when the ratio is above a threshold value [6]. The activator has a relatively weak promoter and therefore scales superlinearly with cell size. Meanwhile, the inhibitor has a relatively strong promoter and therefore scales sublinearly. Our simplified model captures the essential features of cell size control, and the cell can periodically grow and divide, maintaining size homeostasis. We determined the conditions of the stable cell cycle and derived the analytical expression of the cell size. We also provided a new perspective on the linear relationship between cell size and ploidy [18–20]. All of our theoretical predictions were

verified by simulations.

We also proposed a stochastic version of our model in which the division threshold is random in each cell cycle. We found that the cell size at division is uncorrelated with the cell size at birth, known as a sizer [23–25]. Intriguingly, we found that the more differential the cell-size scaling of the cell-cycle regulators is, the narrower the cell-size distribution is. We also extended our model to multiple activators and inhibitors. The cell size becomes larger after one activator is deleted, while it becomes smaller after one inhibitor is deleted, which agrees with experiments [6, 27, 28]. Interestingly, while the mean cell size can change significantly after regulator deletion, the CV of the cell size distribution can be approximately constant, consistent with experiments [27].

Our results support the hypothesis that cells can measure their sizes through the differential scaling of cell-cycle regulatory proteins. Our model is concise and general, not restricted to specific cell-cycle regulators or organisms. Therefore, the conclusions of our work may apply to a wide range of cases. Our model can also be extended by including cell-cycle regulatory networks [29].

In the experiment that exchanged the promoters of *WHI5* and *CLN2*, the cell size of budding yeast increased [6]. We remark that this result is beyond our simple model because the regulation acting on the promoters is not included in our model, and exchanging the promoters may alter the regulatory relationship. For example, Whi5 inhibits the transcription of *CLN2* by binding the SBF complex, and Cln2 can phosphorylate Whi5 and dissociate it from SBF, forming a positive feedback loop [30–32]. Exchanging *WHI5* promoter and *CLN2* promoter may rewire the network. Besides, systematic experiments of exchanging promoters are still lacking, and it is unclear whether the increase in cell size after promoter exchange is a universal phenomenon.

Methods

Details of the gene expression model

We list the variables used in the main text in Table 1. In the gene expression model at the whole-cell level, the time dependence of the protein number follows [8],

$$\frac{\mathrm{d}p_i}{\mathrm{d}t} = \Gamma_{r,i} m_i \frac{F_r c_r}{F_r c_r + K_{r,i}} - \frac{p_i}{\tau_{p,i}}. \tag{7}$$

In particular, we denote the protein number of RNAPs and ribosomes as n and r, and set their index as $i = 1$ and $i = 2$ respectively. $\Gamma_{r,i}$ is the translation initiation rate for a ribosome binding on the ribosome-binding site of mRNAs, c_r is the concentration of total ribosomes in the cytoplasm, $K_{r,i}$ quantifies the binding strength of mRNAs to ribosomes. $\tau_{p,i}$ is the protein lifetime, and F_r is the fraction of free ribosomes in the total pool of ribosomes. F_n and F_r respectively satisfy the following equations due to the conservation of total RNAP and ribosome numbers [8],

$$n(1 - F_n) = \sum_i g_i \left(1 + \frac{\Gamma_{n,i} L_i}{v_n}\right) \frac{F_n c_n}{F_n c_n + K_{n,i}}, \tag{8}$$

$$r(1 - F_r) = \sum_i m_i \left(1 + \frac{\Gamma_{r,i} L_i}{v_r}\right) \frac{F_r c_r}{F_r c_r + K_{r,i}}. \tag{9}$$

The right side of Eq 8 represents RNAPs binding to the promoters or transcribing. Here, L_i is the length of gene i in the unit of codon, and v_n is the RNAP elongation speed. When the number of transcribing RNAPs on one copy of gene i, n_i, does not change with time, we must have $\Gamma_{n,i} P_{b,i} = v_n n_i / L_i$. Here the left side is the number of RNAPs starting transcription per unit time, and the right side is the number of RNAPs

finishing transcribing per unit time. $P_{b,i} \equiv F_n c_n/(F_n c_n + K_{n,i})$ is the probability that the promoter is bound by an RNAP. Therefore, we obtain $n_i = P_{b,i}\Gamma_{n,i}L_i/v_n$, which is included in the right side of Eq 8. Similarly, the right side of Eq 9 represents ribosomes binding to the ribosome-binding sites of mRNAs or translating. v_r is the ribosome elongation speed. For simplicity, we assume that all genes except the activator and the inhibitor share the same transcription MM constant K_n. Heterogeneous $K_{n,i}$ among genes has no significant effects on our results (S5 Fig). All genes except those of RNAPs and ribosomes share the same transcription initiation rate Γ_n (see Details of simulations in Methods). All the mRNAs share the same effective binding strength to ribosomes K_r, the same translational initiation rate Γ_r, and the same mRNA lifetime τ_m. The cell-cycle regulators share the same protein lifetime τ_p and other proteins are nondegradable.

Table 1. A summary of the variables.

Variables	Meaning	Variables	Meaning
$\Gamma_{n,i}$	transcription initiation rate of gene i	$\Gamma_{r,i}$	translation initiation rate of gene i
n	RNAP number	r	ribosome number
c_n	RNAP concentration	c_r	ribosome concentration
F_n	free RNAP fraction	F_r	free ribosome fraction
$K_{n,i}$	transcription MM constant of gene i	$K_{r,i}$	translation MM constant of gene i
v_n	RNAP elongation speed	v_r	ribosome elongation speed
$\tau_{m,i}$	lifetime of mRNAs i	$\tau_{p,i}$	lifetime of protein i
m_i	mRNA number of gene i	p_i	protein number of gene i
g_i	gene copy number of gene i	V	cell volume
L_i	length of gene i	a	ratio between cell volume and nuclear volume
ρ	protein mass per cell volume	n_c	maximum number of RNAPs the entire genome can hold
N	total number of genes	θ	threshold for division

The non-monotonic behavior of $c_{\text{act}}/c_{\text{inh}}$ in one cell cycle

Using Eq 1 about the activator and the inhibitor, we obtain

$$\frac{\mathrm{d}}{\mathrm{d}t}\left(\frac{m_{\text{act}}}{m_{\text{inh}}}\right) = \frac{\Gamma_n F_n c_n}{m_{\text{inh}}(F_n c_n + K_{n,\text{inh}})}\left(\frac{F_n c_n + K_{n,\text{inh}}}{F_n c_n + K_{n,\text{act}}} - \frac{m_{\text{act}}}{m_{\text{inh}}}\right), \tag{10}$$

The left-hand side of Eq 8 decreases monotonically with F_n, while the right-hand side increases monotonically. Therefore, F_n jumps to a smaller value after cell division since n reduces by half after division. According to Eq 10, the drop in F_n turns $\frac{\mathrm{d}}{\mathrm{d}t}\left(\frac{m_{\text{act}}}{m_{\text{inh}}}\right)$ into a negative value, which means that $\frac{m_{\text{act}}}{m_{\text{inh}}}$ starts to decrease. Consequently, the ratio of the production rates of the activator to that of the inhibitor declines, leading to the reduction of $c_{\text{act}}/c_{\text{inh}}$. Then, $\frac{\mathrm{d}}{\mathrm{d}t}\left(\frac{m_{\text{act}}}{m_{\text{inh}}}\right)$ becomes positive again as F_n increases, causing the increase in $c_{\text{act}}/c_{\text{inh}}$.

Derivation of the cell size at birth and the two critical threshold values

Assuming a short lifetime of m_i in Eq 1, we can approximate the mRNA copy number as

$$m_i = \Gamma_{n,i} g_i \tau_m \frac{F_n c_n}{F_n c_n + K_{n,i}}. \tag{11}$$

For those proteins that are not cell-cycle regulators, substituting Eq 11 into Eq 7, we get

$$\frac{\mathrm{d}}{\mathrm{d}t}\left(\frac{p_i}{n}\right) = \frac{\Gamma_r \tau_m \Gamma_{n,n} g_n}{n} \frac{F_n c_n}{F_n c_n + K_n} \frac{F_r c_r}{F_r c_r + K_r} \left(\frac{\Gamma_{n,i} g_i}{\Gamma_{n,n} g_n} - \frac{p_i}{n}\right). \tag{12}$$

At steady state, $\frac{\mathrm{d}}{\mathrm{d}t}\left(\frac{p_i}{n}\right) = 0$. Therefore,

$$\frac{p_i(t)}{n(t)} = \frac{\Gamma_{n,i} g_i}{\Gamma_{n,n} g_n}. \tag{13}$$

The ratio of copy numbers between two proteins is determined by their gene copy numbers and transcription initiation rates.

The total protein mass of the cell is $\sum_i p_i L_i$, in the number of amino acids. The cell size $V(t) = \sum_i p_i(t) L_i / \rho$, where ρ is the ratio between the total protein mass and cell size, which is a constant within our model, consistent with experiments [12–15]. Therefore, the concentration of total RNAPs is approximately constant and can be approximated as

$$c_n = \frac{a n(t)}{V(t)} = \frac{a \rho \Gamma_{n,n} g_n}{\sum_i \Gamma_{n,i} g_i L_i}, \tag{14}$$

Here we have neglected the contribution of the cell-cycle regulators to the total protein mass. Eq 14 shows that the RNAP concentration is independent of ploidy since the double of all genes' copy numbers leaves c_n invariant. Assuming a short lifetime τ_p, using Eq 11 and the quasi-steady state approximation about p_{act} and p_{inh} in Eq 7, we get

$$p_{\mathrm{act}}(t) = \Gamma_n g_{\mathrm{act}} \tau_m \Gamma_r \tau_p \frac{F_n(t) c_n}{F_n(t) c_n + K_{n,\mathrm{act}}} \frac{F_r(t) c_r}{F_r(t) c_r + K_r}, \tag{15}$$

$$p_{\mathrm{inh}}(t) = \Gamma_n g_{\mathrm{inh}} \tau_m \Gamma_r \tau_p \frac{F_n(t) c_n}{F_n(t) c_n + K_{n,\mathrm{inh}}} \frac{F_r(t) c_r}{F_r(t) c_r + K_r}. \tag{16}$$

In the simple case of $g_{\mathrm{act}} = g_{\mathrm{inh}} = 1$, substituting Eqs 15, 16 into the division condition Eq 2 (note that $c_{\mathrm{act}}/c_{\mathrm{inh}} = p_{\mathrm{act}}/p_{\mathrm{inh}}$), we obtain the fraction of free RNAPs at cell division

$$F_{n,d} = \frac{\theta K_{n,\mathrm{act}} - K_{n,\mathrm{inh}}}{(1-\theta) c_n}. \tag{17}$$

We also simplify Eq 8 using the assumption that $K_{n,i} = K_n$ for most genes,

$$n(1 - F_n) \approx n_c \frac{F_n c_n}{F_n c_n + K_n}, \tag{18}$$

where n_c is the maximum number of RNAPs the entire genome can hold [8],

$$n_c = \sum_i g_i \left(1 + \frac{\Gamma_{n,i} L_i}{v_n}\right). \tag{19}$$

Substituting Eq 17 into Eqs 11,18, we get the mRNA copy number and the RNAP number at cell division

$$m_{i,d} = \Gamma_{n,i} g_i \tau_m \frac{\tilde{K}}{(1-\theta) K_n + \tilde{K}}, \tag{20}$$

$$n_d = \frac{n_c c_n (1-\theta) \tilde{K}}{((1-\theta) c_n - \tilde{K})((1-\theta) K_n + \tilde{K})}. \tag{21}$$

Using $n_b = n_d/2$ where n_b is the RNAP number at cell birth and the RNAP concentration Eq 14, we obtain Eq 3. For asymmetrically dividing cells such as budding yeast, we only need to use $n_b = \gamma n_d$ instead, where $\gamma < 1/2$ is the proportion of the cell size that the daughter cell inherits. The condition $0 < F_{n,d} < 1$ in Eq 17 leads to the condition of stable cell cycle Eq 4 so that θ_1 corresponds to $F_{n,d} = 0$ while θ_2 corresponds to $F_{n,d} = 1$. We mathematically prove that the cell cycle is stable against infinitesimal perturbation (S1 Appendix).

Derivation of the amplitude A

Using Eqs 15, 16, the ratio of the activator's concentration to the inhibitor's concentration at a given time t during the cell cycle can be approximated as

$$\frac{c_{\text{act}}(t)}{c_{\text{inh}}(t)} \approx \frac{F_n(t)c_n + K_{n,\text{inh}}}{F_n(t)c_n + K_{n,\text{act}}}. \tag{22}$$

The ratio reaches its minimum when F_n is equal to its minimum value $F_{n,b}$ at cell birth. Therefore,

$$A \approx \theta - \frac{F_{n,b}c_n + K_{n,\text{inh}}}{F_{n,b}c_n + K_{n,\text{act}}}, \tag{23}$$

where $F_{n,b}$ satisfies

$$n_b(1 - F_{n,b}) = n_c \frac{F_{n,b}c_n}{F_{n,b}c_n + K_n}. \tag{24}$$

As θ increases, n_b increases (Eq 21). According to Eq 24, more RNAPs at cell birth generates more free RNAPs, leading to a larger $F_{n,b}$. Therefore, $\frac{F_{n,b}c_n+K_{n,\text{inh}}}{F_{n,b}c_n+K_{n,\text{act}}}$ also increases with θ, consistent with the fact that A first increases and then decreases with θ.

Derivation of $\langle V_b \rangle$ and CV

When $\Delta\theta$ is small, a function f of θ can be approximated as

$$f(\theta) \approx f(\bar{\theta}) + f'(\bar{\theta})(\theta - \bar{\theta}), \quad \theta \in (\bar{\theta} - \Delta\theta, \bar{\theta} + \Delta\theta). \tag{25}$$

Therefore, we can approximate the average and variance of $f(\theta)$ as

$$\mathbb{E}f(\theta) \approx f(\bar{\theta}), \quad \text{Var}f(\theta) \approx \left(f'(\bar{\theta})\right)^2 \sigma^2. \tag{26}$$

Here σ is the standard deviation of θ. Using Eqs 3, 26, we obtain

$$\langle V_b \rangle = \mathbb{E}V_b \approx \frac{a n_c (1-\bar{\theta})\bar{\tilde{K}}}{2((1-\bar{\theta})c_n - \bar{\tilde{K}})((1-\bar{\theta})K_n + \bar{\tilde{K}})}, \tag{27}$$

$$\text{CV} = \frac{\sqrt{\text{Var}V_b}}{\mathbb{E}V_b} \approx \frac{(K_{n,\text{act}} - K_{n,\text{inh}})\left((1-\bar{\theta})^2 c_n K_n + \bar{\tilde{K}}^2\right)\sigma}{(1-\bar{\theta})\bar{\tilde{K}}((1-\bar{\theta})c_n - \bar{\tilde{K}})((1-\bar{\theta})K_n + \bar{\tilde{K}})}, \tag{28}$$

where $\bar{\tilde{K}} \equiv \bar{\theta}K_{n,\text{act}} - K_{n,\text{inh}}$.

The condition of robust cell division for the stochastic model

We denote θ_k as the division threshold value of the k-th cell cycle. Given $\bar{\theta}$ and $\Delta\theta$, to ensure robust division, we require that the minimum value of the activator-to-inhibitor

ratio in the k-th cell cycle $\theta_{k-1} - A(\theta_{k-1})$ is smaller than θ_k, where $A(\theta_{k-1})$ is the amplitude of the k-th cell cycle, which is a function of θ_{k-1}. This condition must hold for any θ_{k-1} and θ_k. Therefore,

$$\max\{\theta - A(\theta)\} < \min\{\theta\}, \quad \theta \in (\bar{\theta} - \Delta\theta, \bar{\theta} + \Delta\theta). \tag{29}$$

Because $\theta - A(\theta)$ increases with $F_{n,b}$ (see Eq 23) and $F_{n,b}$ increases with θ, $\theta - A(\theta)$ increases with θ. Therefore,

$$\max\{\theta - A(\theta)\} = (\bar{\theta} + \Delta\theta) - A(\bar{\theta} + \Delta\theta). \tag{30}$$

Substituting Eq 30 into Eq 29, we obtain Eq 6.

Details of simulations

All simulations were done in MATLAB (version R2021b). We summarize some of the parameters used in simulations in Table S1 of S1 Appendix. To find reasonable values of $\Gamma_{n,i}$, we first set $n_c = 10^4$ as in [8]. Assuming the number of RNAPs is about 10% of ribosomes i.e. $n = 0.1r$, from Eq 13 we get

$$\Gamma_{n,n} = \frac{0.1\Gamma_{n,r} g_r}{g_n}. \tag{31}$$

Assuming the length of genes except those of RNAPs and ribosomes is L, from Eq 19 we get,

$$\Gamma_n = \frac{(n_c - \sum_i g_i)v_n - \Gamma_{n,n} g_n L_n - \Gamma_{n,r} g_r L_r}{L \sum_{i>2} g_i}. \tag{32}$$

Substituting Eq 11 into Eq 9, we get

$$\frac{F_r c_r}{F_r c_r + K_r} \approx \frac{r(1 - F_r)}{\tau_m \frac{F_n c_n}{F_n c_n + K_n} \sum_i \Gamma_{n,i} g_i \left(1 + \frac{\Gamma_r L_i}{v_r}\right)}. \tag{33}$$

Substituting Eqs 11,33 into Eq 7 for r, we find the growth rate as

$$\mu = \frac{1}{r}\frac{\mathrm{d}r}{\mathrm{d}t} \approx \frac{\Gamma_{n,r} g_r \Gamma_r (1 - F_r)}{\sum_i \Gamma_{n,i} g_i \left(1 + \frac{\Gamma_r L_i}{v_r}\right)}. \tag{34}$$

In this work, we set the attempted growth rate $\mu = (\ln 2)/2$ h^{-1}. Substituting Eqs 31,32 to Eq 34, and letting $F_r = 0$, which is merely a numerical convenience, we obtain

$$\Gamma_{n,r} = \frac{\mu v_n (n_c - \sum_i g_i)\left(1 + \frac{\Gamma_r L}{v_r}\right)}{g_r(\Gamma_r L - \mu(1.1L - 0.1L_n - L_r))}, \tag{35}$$

from which we find $\Gamma_{n,n}$ and Γ_n.

Our theoretical results do not rely on the initial values of simulations, but appropriate initial values make it easier to reach the steady state. We first set an attempted cell volume V_0, and then we get $n(0) = c_n V_0/a$ where c_n is calculated using Eq 14. Finally, we determine $p_i(0)$ $(i > 1)$ using Eq 13 and $m_i(0)$ using Eq 11. After symmetric division, mRNAs and proteins are equally distributed to the two daughter cells. We also have a requirement on the minimum cell-cycle duration to avoid cell division immediately after cell birth. Before we take the simulation results, we run the simulations for several generations to ensure that the cell reaches a steady state.

Supporting information

S1 Appendix. Supplementary information.

S1 Fig. The free RNAP fraction F_n drops abruptly at division while the free ribosome fraction F_r does not (related to Fig 1). $K_{n,\mathrm{act}} = 12000\ \mu\mathrm{m}^{-3}$, $K_{n,\mathrm{inh}} = 4000\ \mu\mathrm{m}^{-3}$, and $\theta = 0.7$.

S2 Fig. Comparison between theories and simulations of the stochastic model (related to Fig 4). (A) $\langle V_b \rangle$ decreases with $K_{n,\mathrm{inh}}$, and the CV of V_b increases with $K_{n,\mathrm{inh}}$. $K_{n,\mathrm{act}} = 12000\ \mu\mathrm{m}^{-3}$, $\bar{\theta} = 0.7$, $\Delta\theta = 0.1$. (B) Illustration of the tendency in (A). The intersection of c_{inh} and $c_{\mathrm{act}}/\bar{\theta}$ (red solid line) determines $\langle V_d \rangle$. The intersections of c_{inh} with $c_{\mathrm{act}}/(\bar{\theta} - \Delta\theta)$ and $c_{\mathrm{act}}/(\bar{\theta} + \Delta\theta)$ (red dashed lines) set the range of V_d. If $K_{n,\mathrm{inh}}$ decreases, the number of inhibitor becomes more sublinear as a function of cell size and c_{inh} shifts to the green line with lower transparency. Therefore, $\langle V_d \rangle$ increases while the CV of V_d decreases. Since $V_b = V_d/2$, the same conclusions apply to V_b.

S3 Fig. The standard deviation (STD) of cell size vs. the mean cell size at budding of various budding yeast mutants. Each point represent a budding yeast mutant with one particular gene belonging to the positive or negative regulator category [27] knocked out, and the red line is the linear fit using the equation $y = bx$. The R^2 is about 0.92, indicating that the STD is nearly proportional to the mean. Thus, after deleting an activator or inhibitor, the mean cell size at budding can change a lot while the CV of cell size at budding remains roughly the same. The data are from Dataset S3 of [27].

S4 Fig. Simulations of multiple regulators (related to Fig 5). (A) $|\delta_{\langle V_b \rangle}|$ and $|\delta_{\mathrm{CV}}|$ vs. $\bar{\theta}$ after deleting one inhibitor. The dash lines mark the range of $\bar{\theta}$ that enables WT, *activator*Δ and *inhibitor*Δ to divide. $K_{n,\mathrm{act}} = 12000\ \mu\mathrm{m}^{-3}$, $K_{n,\mathrm{inh}} = 4000\ \mu\mathrm{m}^{-3}$, $\Delta\theta = 0.1$. (B) The deletion of one inhibitor shifts the total concentration of all inhibitors ($\sum c_{\mathrm{inh}}$) downward while the total concentration of all activators ($\sum c_{\mathrm{act}}$) remain the same. This leads to a change in $\langle V_d \rangle$ while the CV of V_d is almost the same.

S5 Fig. The model with heterogeneous $K_{n,i}$ among genes. We simulate a model in which the transcription MM constants are heterogeneous among genes, and compare the simulations with theoretical predictions. (A) V_b vs. $\tilde{K}$. $\theta = 0.8$. (B) V_b vs. θ. (C) A vs. θ. In (B-C), $K_{n,\mathrm{act}} = 12000\ \mu\mathrm{m}^{-3}$, $K_{n,\mathrm{inh}} = 4000\ \mu\mathrm{m}^{-3}$. In all panels, the dashed lines mark the two predicted critical threshold values. $K_{n,i}$ follows a lognormal distribution with the mean $K_n = 6000\ \mu\mathrm{m}^{-3}$ and the CV equal to 0.5.

S6 Fig. The modified model with gene replication. (A) The concentration of the activator c_{act} and inhibitor c_{inh}, (B) $c_{\mathrm{act}}/c_{\mathrm{inh}}$ and (C) the cell volume V change periodically. (D) The free RNAP fraction F_n drops abruptly at gene replication while the free ribosome fraction F_r does not. In (A-D), the dashed lines mark cell division, and $\theta = 0.7$. (E) Simulations and theoretical predictions of V_b vs. θ. In this figure, $K_{n,\mathrm{act}} = 12000\ \mu\mathrm{m}^{-3}$, $K_{n,\mathrm{inh}} = 4000\ \mu\mathrm{m}^{-3}$, $T_M = 60$ min.

S7 Fig. The model of nondegradable inhibitor. (A) Simulations and theoretical predictions of V_b vs. θ in the deterministic model. The dashed line marks the predicted critical points θ_1. (B) Illustration of two critical division thresholds. Note that c_{act} and θc_{inh} may have two intersections. Only the intersection on the left determines V_d,

because as the cell volume increases, $c_{\mathrm{act}}/c_{\mathrm{inh}}$ must rise to θ. Beyond two critical points (dashed lines), there is no intersection. (C) V_d vs. V_b in the stochastic model. (D) ΔV vs. V_b. (E) T_D vs. V_b. In (C-E), we simulate the stochastic model and each point represents one cell cycle. The Pearson correlation coefficient R and slope of the linear regression are shown in the title. $\bar{\theta} = 0.018$. (F) Given a fixed θ, V_b increases after deleting one activator and decreases after deleting one inhibitor. The dashed lines mark the range of θ that simultaneously allows WT, *activator*Δ and *inhibitor*Δ to divide. (G) In the stochastic model, $\langle V_b \rangle$ increases after deleting one activator and decreases after deleting one inhibitor. The CV of V_b changes mildly after deleting one regulator. (H) $|\delta_{\langle V_b \rangle}|$ and $|\delta_{\mathrm{CV}}|$ vs. $\bar{\theta}$ after deleting one activator. (I) $|\delta_{\langle V_b \rangle}|$ and $|\delta_{\mathrm{CV}}|$ vs. $\bar{\theta}$ after deleting one inhibitor. In (G-I), the dashed lines mark the range of $\bar{\theta}$ that simultaneously allows WT, *activator*Δ and *inhibitor*Δ to divide. $g_{\mathrm{act}} = g_{\mathrm{inh}} = 10$. In (A, C-E, F-I), $K_{n,\mathrm{act}} = 12000\ \mu\mathrm{m}^{-3}$, $K_{n,\mathrm{inh}} = 4000\ \mu\mathrm{m}^{-3}$. In (C-E, G-I), $\Delta\theta = 0.0018$.

Acknowledgments

We thank Lingyu Meng, Qirun Wang, Yiyang Ye, and Yichen Yan for helpful discussions related to this work. The research was funded by National Key R&D Program of China (2021YFF1200500) and supported by grants from Peking-Tsinghua Center for Life Sciences.

References

1. Neurohr GE, Terry RL, Lengefeld J, Bonney M, Brittingham GP, Moretto F, et al. Excessive Cell Growth Causes Cytoplasm Dilution And Contributes to Senescence. Cell. 2019;176(5):1083–1097.e18. doi:10.1016/j.cell.2019.01.018.

2. Lanz MC, Zatulovskiy E, Swaffer MP, Zhang L, Ilerten I, Zhang S, et al. Increasing cell size remodels the proteome and promotes senescence. Molecular Cell. 2022;82(17):3255–3269.e8. doi:10.1016/j.molcel.2022.07.017.

3. Elowitz MB, Levine AJ, Siggia ED, Swain PS. Stochastic gene expression in a single cell. Science. 2002;297(5584):1183–1186. doi:10.1126/science.1070919.

4. Paulsson J. Models of stochastic gene expression. Physics of Life Reviews. 2005;2(2):157–175. doi:10.1016/j.plrev.2005.03.003.

5. Lin J, Amir A. Disentangling Intrinsic and Extrinsic Gene Expression Noise in Growing Cells. Phys Rev Lett. 2021;126:078101. doi:10.1103/PhysRevLett.126.078101.

6. Chen Y, Zhao G, Zahumensky J, Honey S, Futcher B. Differential scaling of gene expression with cell size may explain size control in budding yeast. Molecular Cell. 2020;78(2):359–370.e6. doi:10.1016/j.molcel.2020.03.012.

7. Xie S, Swaffer M, Skotheim JM. Eukaryotic Cell Size Control and Its Relation to Biosynthesis and Senescence. Annual review of cell and developmental biology. 2022;38:291–319. doi:10.1146/annurev-cellbio-120219-040142.

8. Wang Q, Lin J. Heterogeneous recruitment abilities to RNA polymerases generate nonlinear scaling of gene expression with cell volume. Nature Communications. 2021;12(1):6852. doi:10.1038/s41467-021-26952-y.

9. Christiano R, Nagaraj N, Fröhlich F, Walther TC. Global Proteome Turnover Analyses of the Yeasts S.cerevisiae and S.pombe. Cell Reports. 2014;9(5):1959–1965. doi:10.1016/j.celrep.2014.10.065.

10. Lin J, Amir A. Homeostasis of protein and mRNA concentrations in growing cells. Nature Communications. 2018;9(1):4496. doi:10.1038/s41467-018-06714-z.

11. Milo R, Phillips R. Cell biology by the numbers. New York: Garland Science; 2015.

12. Crissman HA, Steinkamp JA. Rapid, simultaneous measurement of DNA, protein, and cell volume in single cells from large mammalian cell populations. Journal of Cell Biology. 1973;59(3):766–771. doi:10.1083/jcb.59.3.766.

13. You C, Okano H, Hui S, Zhang Z, Kim M, Gunderson CW, et al. Coordination of bacterial proteome with metabolism by cyclic AMP signalling. Nature. 2013;500(7462):301–306. doi:10.1038/nature12446.

14. Bryan AK, Hecht VC, Shen W, Payer K, Grover WH, Manalis SR. Measuring single cell mass, volume, and density with dual suspended microchannel resonators. Lab Chip. 2014;14:569–576. doi:10.1039/C3LC51022K.

15. Basan M, Zhu M, Dai X, Warren M, Sévin D, Wang YP, et al. Inflating bacterial cells by increased protein synthesis. Molecular Systems Biology. 2015;11(10). doi:10.15252/msb.20156178.

16. Jorgensen P, Edgington NP, Schneider BL, Rupeš I, Tyers M, Futcher B. The size of the nucleus increases as yeast cells grow. Molecular Biology of the Cell. 2007;18(9):3523–3532. doi:10.1091/mbc.E06-10-0973.

17. Neumann FR, Nurse P. Nuclear size control in fission yeast. Journal of Cell Biology. 2007;179(4):593–600. doi:10.1083/jcb.200708054.

18. Fankhauser G. Maintenance of normal structure in heteroploid salamander larvae, through compensation of changes in cell size by adjustment of cell number and cell shape. Journal of Experimental Zoology. 1945;100(3):445–455. doi:10.1002/jez.1401000310.

19. Mortimer RK. Radiobiological and genetic studies on a polyploid series (haploid to hexaploid) of Saccharomyces cerevisiae. Radiation research. 1958;9(3):312–326. doi:10.2307/3570795.

20. Nurse P. The genetic control of cell volume. In: Cavalier-Smith T, editor. The Evolution of Genome Size. John Wiley and Sons; 1985. p. 185–196.

21. Marshall WF, Young KD, Swaffer M, Wood E, Nurse P, Kimura A, et al. What determines cell size? BMC Biology. 2012;10:101. doi:10.1186/1741-7007-10-101.

22. Wood E, Nurse P. Sizing up to Divide: Mitotic Cell-Size Control in Fission Yeast. Annual Review of Cell and Developmental Biology. 2015;31:11–29. doi:10.1146/annurev-cellbio-100814-125601.

23. Turner JJ, Ewald JC, Skotheim JM. Cell size control in yeast. Current Biology. 2012;22(9):R350–R359. doi:10.1016/j.cub.2012.02.041.

24. Facchetti G, Chang F, Howard M. Controlling cell size through sizer mechanisms. Current Opinion in Systems Biology. 2017;5:86–92. doi:10.1016/j.coisb.2017.08.010.

25. Xie S, Skotheim JM. A G1 Sizer Coordinates Growth and Division in the Mouse Epidermis. Current Biology. 2020;30(5):916–924.e2. doi:10.1016/j.cub.2019.12.062.

26. Serbanescu D, Ojkic N, Banerjee S. Nutrient-Dependent Trade-Offs between Ribosomes and Division Protein Synthesis Control Bacterial Cell Size and Growth. Cell Reports. 2020;32(12):108183. doi:10.1016/j.celrep.2020.108183.

27. Soifer I, Barkai N. Systematic identification of cell size regulators in budding yeast. Molecular Systems Biology. 2014;10(11):761. doi:10.15252/msb.20145345.

28. Jorgensen P, Nishikawa JL, Breitkreutz BJ, Tyers M. Systematic identification of pathways that couple cell growth and division in yeast. Science. 2002;297(5580):395–400. doi:10.1126/science.1070850.

29. Bertoli C, Skotheim JM, De Bruin RAM. Control of cell cycle transcription during G1 and S phases. Nature Reviews Molecular Cell Biology. 2013;14(8):518–528. doi:10.1038/nrm3629.

30. De Bruin RAM, McDonald WH, Kalashnikova TI, Yates III J, Wittenberg C. Cln3 activates G1-specific transcription via phosphorylation of the SBF bound repressor Whi5. Cell. 2004;117(7):887–898. doi:10.1016/j.cell.2004.05.025.

31. Costanzo M, Nishikawa JL, Tang X, Millman JS, Schub O, Breitkreuz K, et al. CDK activity antagonizes Whi5, an inhibitor of G1/S transcription in yeast. Cell. 2004;117(7):899–913. doi:10.1016/j.cell.2004.05.024.

32. Skotheim JM, Di Talia S, Siggia ED, Cross FR. Positive feedback of G1 cyclins ensures coherent cell cycle entry. Nature. 2008;454(7202):291–296. doi:10.1038/nature07118.